Medical Image Segmentation Using Phase-Field Method based on GPU Parallel Programming

Albertus Joko Santoso*, and Pranowo, *Member, IAENG*

***Abstract*—The use of a Phase Field method for medical image segmentation is proposed in this paper. The Allen-Cahn equation, a mathematical model equation, is used in this method. The Finite Difference method is used for numerical discretization of model equations and semi-algebraic equations integrated over time using the second-order Runge-Kutta method. Numerical algorithms are implemented into computer programming using the serial and parallel C programming language based on GPU CUDA. Based on image segmentation calculations, the Phase Field method has high accuracy. It is indicated by the Jaccard Index and Dice Similarity values that are close to one. The range of Jaccard Index values is 0.859 - 0.952, while the Dice Similarity value range is 0.926 - 0.976. In addition, it is shown that parallel programming with GPU CUDA can accelerate 45.72 times compared to serial programming.**

***Index Terms*—Medical Image, Segmentation, Phase Field, GPU, Parallel Programming**

I. Introduction

IMAGE segmentation is part of image analysis which is fundamental and essential. Segmentation is used to separate multiple objects in an image.The basic assumption in the segmentation process is that each object in the image contains different image intensities and has a constant value. Relatively sharp and visible edges limit these objects. The segmentation process looks for these boundaries and groups things into many areas with a homogeneous image intensity.

Currently, researchers are intensively developing digital image segmentation methods to continuously increase the performance of the segmentation method [1][2][3]. The method that has received serious attention is the segmentation method based on the evolution of curves that can trace the boundaries of objects on the image to be separated. The Active Contour method, also known as Snakes [4], is the embryo of the curve evolution-based method. This method is quite efficient but sensitive to the initial conditions of the curve and difficult to apply to images containing separate objects. Osher and Sethian's proposed level set method [5} succeeded in improving the weaknesses of the Active Contour method. The evolutionary movement of the Level Set curve towards the object boundary is based on the gradient of the pixel intensity value that is on the object boundary. In contrast, not all object boundaries can be determined using a pixel intensity gradient.

Chan and Vese [6] proposed a Mumford-Shah [7] method, function to enhance the performance of the Level Set method. The method proposed can detect objects whose boundaries cannot be calculated using a pixel gradient. The proposed method by Chan and Vese became known as Chan-Vese method and continued to be developed and expanded into various kinds of segmentation for medical images. Maška et al. [8] carried out the segmentation process and shape tracking of cell movement using the Chan-Vese method. Before segmentation is carried out, the digital image is filtered first and then clustered. The proposed method can increase 9 % accuracy compared to the conventional Level Set method. Chen, Liu, and Zhu [9] proposed the self-adaptive Chan and Vese (SACV) level set method for segmenting the iris and pupil of the eye. The disturbance in the segmentation process due to the presence of eyelashes and eyelids can be overcome. The proposed method is accurate and robust against various kinds of noise. Rajalaxmi and Nirmala [10] improve the initialization performance of the Chan-Vese method by proposing the use of the Endo Fitting Curve to initialize calculations. The proposed method can reduce computation time and can provide segmentation results on Echocardiography images. Femina and Raajagopalan [11] combined a meta-heuristic algorithm called global pollination-based CAT swarm (GPCATS) with the Chan-Vese method. The purpose of using the GPCATS method is to avoid the level set curve getting stuck in an undesirable area because that area is a local minimum. The calculations show that the proposed method outperforms the active contour method in determining the boundaries of an object in an image.

As mentioned above, efforts to improve the performance of both the Level set and Chan-Vese methods are continuously being made. Beneš, Chalupecký, and Mikula [12] suggest using the phase-field method by directly applying the Allen-Cahn equation for segmentation. Kay and Tomasi [13] used the phase-field method for colour image segmentation with the Finite Element (FE) method discretization. The FE method is relatively difficult and requires a large matrix inversion. In the study, the inversion of the matrix was carried out iteratively with the multigrid

Manuscript received February 3, 2021; revised December 3, 2021. This research was supported by funds from Universitas Atma Jaya Yogyakarta, based on a letter of assignment (No. : 025/In-Pen/LPPM/I/2020).

Albertus Joko Santoso is a lecturer at the Faculty of Industrial Technology, Universitas Atma Jaya Yogyakarta, Indonesia. (Corresponding Author, e-mail: albjoko@staff.uajy.ac.id).

Pranowo is a lecturer at the Faculty of Industrial Technology,Universitas Atma Jaya Yogyakarta, Indonesia. (e-mail: pranowo@uajy.ac.id).

method. Li and Kim [14,15,16] proposed replacing the calculation of the length of the curve in the Mumford-Shah function with the Allen Chan equation. An implicit splitting Finite Difference scheme then solved the equation that was formed. The equation for the linear system that was created was solved by using the Multigrid method. The proposed method for image segmentation is efficient and robust. Thasneem, Sathik, and Mehaboobathunnisa [17] applied the method developed by Li and Kim [14,15] for segmenting 3-dimensional medical images. The images are the combination of hundreds of 2-dimensional medical images. The calculation results show that using the phase-field method can increase the accuracy of the calculation of 3-D image segmentation. Lee and Lee [18] For image segmentation, Allen Cahn's equation was modified with a Laplacian fractional. The segmentation results show that the Laplacian fractional accuracy outperforms the standard Allen Cahn equation.

An effort to speed up the computation time of the phase-field method was carried out by utilizing parallel Graphical Processing Units (GPU) programming. However, the effort was not used for image segmentation but for modelling the formation of alloy material. Zhu et al. [19] implemented a phase-field method using parallel GPU programming to simulate dendrite growth. As a result, computing time can be accelerated up to 56 times. Yang, Xu, and Liu [20] simulated the microstructural changes in the superalloy nickel solidification process. Lee and Chang [21] studied the effect of magnetic ordering on the spinodal decomposition of the Fe-Cr system.

Based on the description above, no other researchers have used parallel GPU programming for image segmentation using the phase-field method. Therefore, this paper proposes using the Phase Field method developed by Li and Kim [14] using the second-order Runge-Kutta method and parallel programming based on GPU to speed up computation time.

II. THEORY BACKGROUND

In this paper, the phase-field function $\phi(x, y)$ represents the segmenting curve C for a given normalized image f_0. The phase-field function $\phi(x, y)$ is defined as:

$$\phi(x,y)=\begin{cases}>0 & \text{if } (x,y)\in \text{inside } C\\ =0 & \text{if } (x,y)\in C\\ <0 & \text{if } (x,y)\in \text{outside } C\end{cases} \tag{1}$$

The range of phase-field value is $-1 \le \phi \le 1$, where ($\phi = 0$) is equal to the segmenting curve C.

The evolution of the phase-field function is governed by the modified Allen-Cahn equation, which is derived by Li dan Kim [14,15]:

$$\frac{\partial \phi}{\partial t}=-\frac{\phi^3-\phi}{\varepsilon^2}+\frac{\partial^2\phi}{\partial x^2}+\frac{\partial^2\phi}{\partial y^2}+\lambda\left(\left(1+\phi\right)\left(f_0-c_1\right)^2+\left(1-\phi\right)\left(f_0-c_2\right)^2\right) \tag{2}$$

$$c_1=\frac{\int_\Omega f_0(x,y)(1+\phi)dxdy}{\int_\Omega f(1+\phi)dxdy} \quad \text{and} \quad c_2=\frac{\int_\Omega f_0(x,y)(1-\phi)dxdy}{\int_\Omega f(1-\phi)dxdy} \tag{3}$$

The Ω is the image domain, ε is the gradient energy parameter, λ is the positive parameter, c_1 and c_2 are the averages of the pixel values f_0 in the regions ($\phi > 0$) and ($\phi < 0$). It is assumed that the phase-field functions as time-dependent variables. It can grow or shrink. Once the steady-state is reached, the zero level of the function ($\phi = 0$) becomes the curve that separates the segmented object from the background image.

The modified Allen Cahn, i.e., equation 1, is discretized using the finite difference method in the two-dimensional domain. Let $N_x \times N_y$ denotes the image resolution, h is the uniform mesh size, (i, j) is the pixel position index, Δt denotes the time step size, and n is the time step level. Then, the semi-algebraic equation is integrated using the second-order Runge-Kutta [22] method as follow:

$$\phi^{n+1}=\phi^n+\frac{\Delta t}{2}\left(K_1+K_2\right) \tag{3a}$$

$$K_1=-\frac{\left(\phi_{i,j}^n\right)^3-\phi_{i,j}^n}{\varepsilon^2}+\frac{\phi_{i+1,j}^n-2\phi_{i,j}^n-\phi_{i-1,j}^n}{h^2}+\frac{\phi_{i,j+1}^n-2\phi_{i,j}^n-\phi_{i,j-1}^n}{h^2}+\lambda\left(\left(1+\phi_{i,j}^n\right)\left(f_0-c_1^n\right)^2+\left(1-\phi_{i,j}^n\right)\left(f_0-c_1^n\right)^2\right) \tag{3b}$$

$$\phi^{n+1/2}=\phi^n+K_1\Delta t \tag{3c}$$

$$K_2=-\frac{\left(\phi_{i,j}^{n+1/2}\right)^3-\phi_{i,j}^{n+1/2}}{\varepsilon^2}+\frac{\phi_{i+1,j}^{n+1/2}-2\phi_{i,j}^{n+1/2}-\phi_{i-1,j}^{n+1/2}}{h^2}+\frac{\phi_{i,j+1}^{n+1/2}-2\phi_{i,j}^{n+1/2}-\phi_{i,j-1}^{n+1/2}}{h^2}+\lambda\left(\left(1+\phi_{i,j}^{n+1/2}\right)\left(f_0-c_1^{n+1/2}\right)^2+\left(1-\phi_{i,j}^{n+1/2}\right)\left(f_0-c_2^{n+1/2}\right)^2\right) \tag{3d}$$

III. PARALEL GPU IMPLEMENTATION

In this paper, the CUDA (Compute Unified Device Architecture), which NVIDIA creates, is used as the parallel computing platform. By using the CUDA platform, one can enable GPU for general purpose processing. From a programming standpoint, the GPU device makes use of the kernel to run a command n times in parallel on the GPU device. Several n-thread handle the execution. Threads which are the backbone of GPU parallelization, are organized into grids and blocks. That way of organizing the thread is useful for accessing many threads. The detailed information on thread organization can be found in Cheng et al. [23]. Suban, et.al [24] said the kernel is a C subprogram that is executed on the GPU device and is invoked by the host (CPU). The following is the working sequence interaction between the host (CPU) and device (GPU). The host sends the kernel and thread to the GPU asynchronously and waits for parallel execution in the GPU to complete before moving on to the next seed. The GPU similar algorithm for the phase-field segmentation process is

described in Fig. 1. A solid box represents the general cooperation of CPU and GPU and the numerical solution of the phase-field function implemented on GPU.

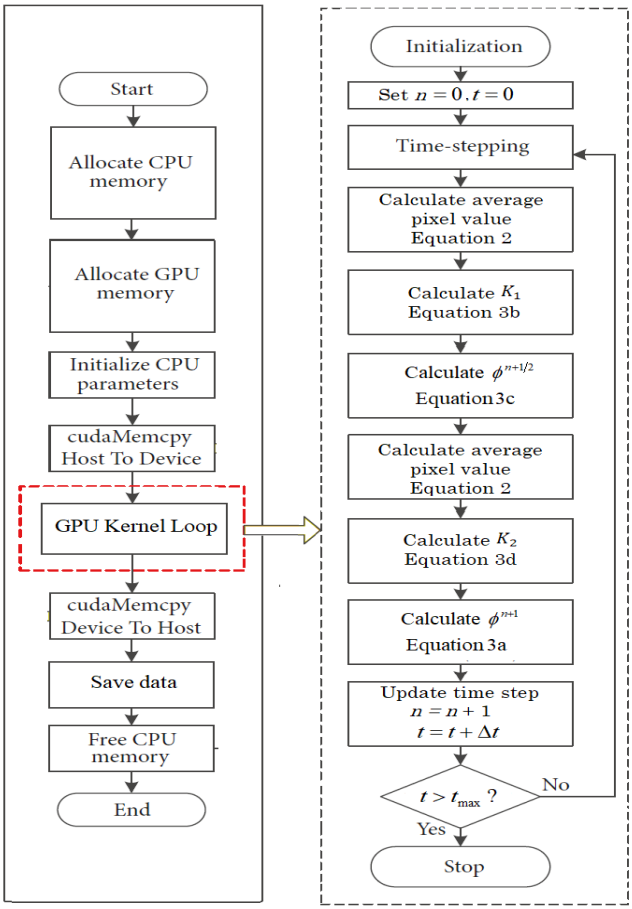

Fig. 1. Parallel GPU algorithm of the Phase Field method, adopted from [25].

IV. RESULT AND DISCUSSION

Our proposed method is tested using authentic grayscale medical images provided by Nanfang Hospital and General Hospital, Tianjin Medical University [26, 27] and images obtained from https://github.com/edvardskrumins/-aneurysm/tree/master/images. The real image f is normalized as

$$f_0 = \frac{f - f_{\min}}{f_{\max} - f_{\min}} \tag{4}$$

Where $f_{\min}$ and $f_{\max}$ are the maximum and minimum intensities of the real images. To achieve the value of the Phase Field function distributed smoothly across the interfacial region; therefore, the value of the gradient energy parameter ε is determined as follows:

$$\varepsilon = \frac{2h}{2\sqrt{2}\tanh^{-1}(0.9)} \tag{5}$$

The initial condition of the phase-field function is defined as follows:

$$\phi = \tanh\left(5\left(2f_0 - 1 - \phi_s\right)\right) \tag{6}$$

Where ϕ_s is the approximation value of the phase-field function of segmented objects, the mesh size h = 0.01, time step size $\Delta t = 2 \times 10^{-6}$, $\lambda = 10^5$ and final time = $200\Delta t$ are used for all calculations.

The Jaccard Index and Dice Similarity are used to evaluate the segmentation results [28]. Jaccard index is defined as:

$$J(A,B) = \frac{|A \cap B|}{|A \cup B|} \tag{7}$$

Furthermore, the Dice Similarity is defined as:

$$D(A,B) = \frac{2|A \cap B|}{|A| + |B|} \tag{8}$$

where A and B are the images to be compared.

In the first experiment, the segmentation results obtained using serial CPU dan parallel GPU programming are compared. The size of the images is 1024 × 1024 pixels. The value of the Jaccard index is J = 0.994, and the value of Dice Similarity D = 0.997. Fig. 2 depicts the segmentation results obtained using both programming methods.

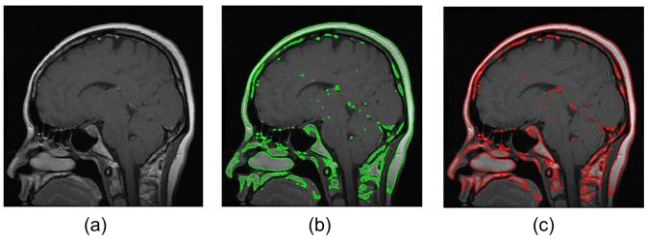

Fig. 2. Comparison of segmentation results using CPU and GPU programming. Original image (a), segmentation using serial CPU programming (b), and segmentation using parallel GPU Programming (c).

The results of the segmentation between both programming methods have an excellent coincidence.

For the second experiment, images with various resolution sizes are used to test the execution speed of CPU serial and parallel GPU programming. The size of images is 512×512 pixels, 1024×1024 pixels, 1792×1792 pixels, 2048×2048 pixels, and 3072×4096 pixels. Fig. 3.1 – Fig. 3.5 show the original image, the segmented contour, and the Phase Field's surface, using parallel GPU programming.

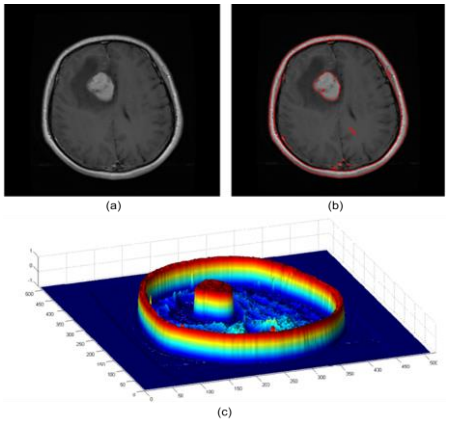

Fig. 3.1. The results of segmentation medical image sized 512×512 pixels, the original image (a), the contour of the segmentation result using the GPU (b), the the surface of phase-field (c).

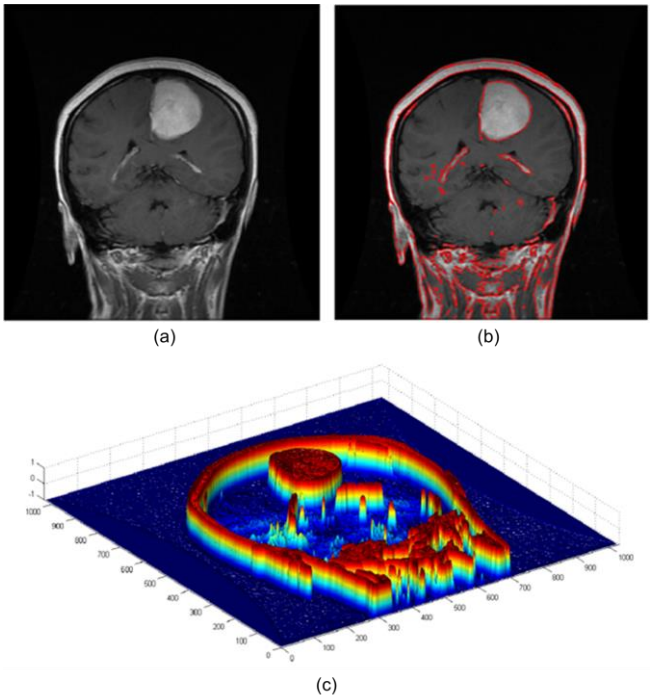

Fig. 3.2. The results of segmentation medical image sized 1024 x 1024 pixels, the original image (a), the contour of the segmentation result using the GPU (b), the surface of phase-field (c).

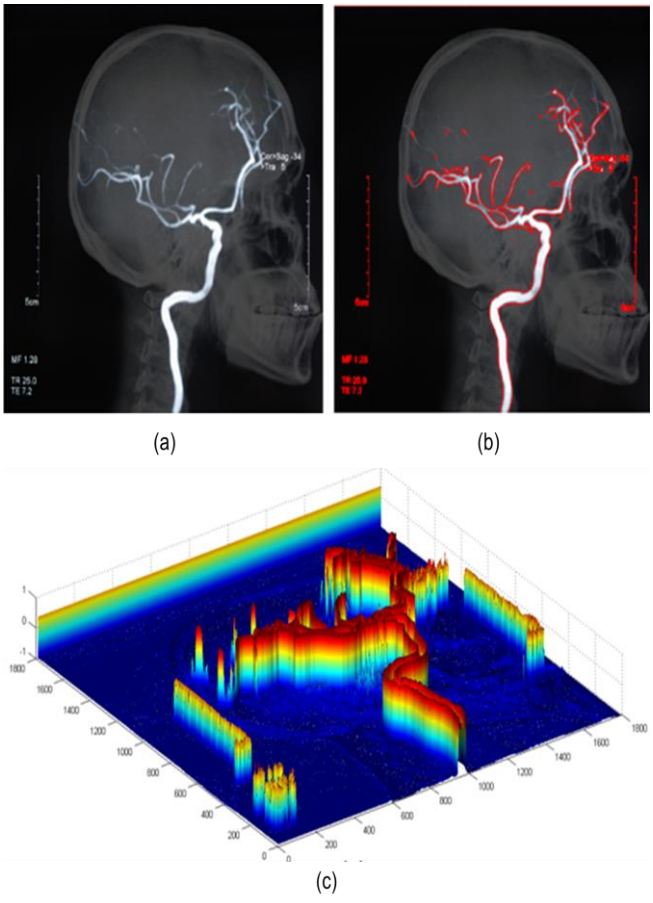

Fig. 3.3. The results of segmentation medical image sized 1792×1792 pixels, the original image (a), the contour of the segmentation result using the GPU (b), the surface of phase-field (c).

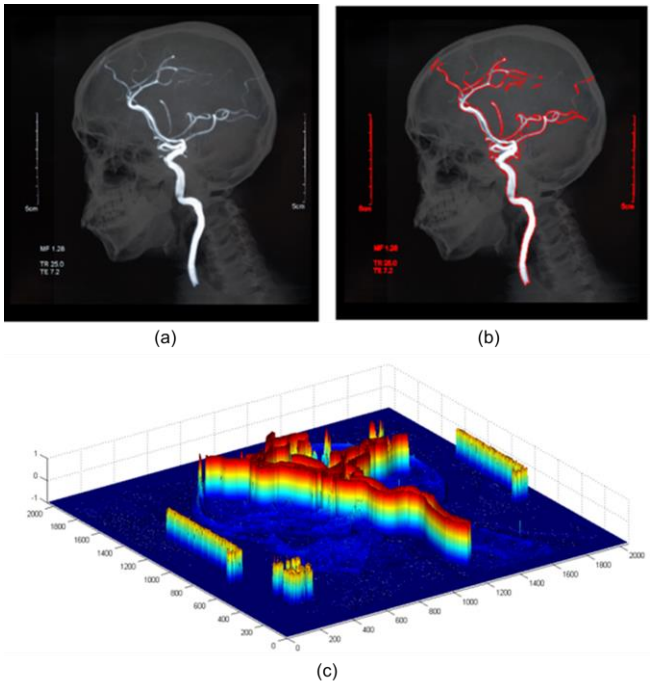

Fig. 3.4. The results of segmentation medical image sized 2048×2048 pixels, the original image (a), the contour of the segmentation result using the GPU (b), the surface of phase-field (c).

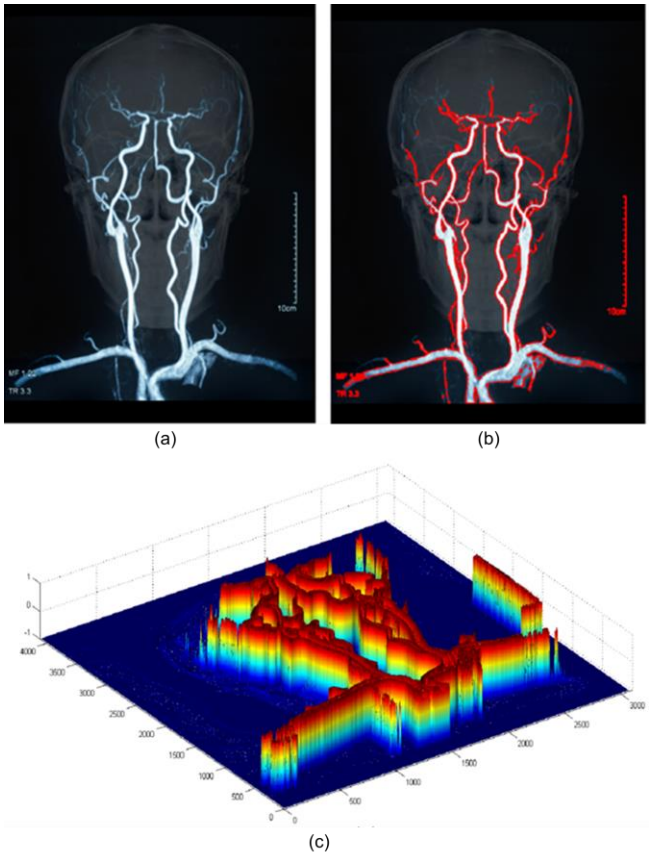

Fig. 3.5. The results of segmentation medical image sized 3072×4096 pixels, the original image (a), the contour of the segmentation result using the GPU (b), the surface of phase-field (c).

The execution time for the serial and parallel segmentation processes is shown in Table I. According to the data in Table I, parallel programming with GPU CUDA can significantly enhance the speed. Specifically, when the image resolution is 3072 × 4096 pixels, programming with GPU has a processing speed that is 45.72 times speedier

than serial programming with a CPU. Increasing image resolution tends to lengthen execution time, whether CPU or GPU, however, the speed-up also increases.

TABLE I
SPEED COMPARISON RESULTS

Image resolution (pixels)	Time (ms)		Speed-up (× times)
	Serial CPU	Parallel GPU	
512×512	2662.33	143.42	18.56
1024×1024	10931.37	318.72	34.30
1792x1792	34439.03	765.73	44.98
2048×2048	44667.74	998.58	44.73
3072×4096	129365.55	2829.81	45.72

Brain tumor segmentations are used as third experiments. The segmentation results are validated using the ground truth images of the tumor. Post-processing of the segmentation results is needed to obtain the tumor segmentation. In this work, the post-processing uses the *bwareaopen* command in Matlab to remove segmented objects other than the tumor. Fig. 4.1 – Fig. 4.2 shows the results of Meningioma tumor segmentation, and Fig. 5.1 – Fig. 5.2 shows the results of Pituitary tumor segmentation. Each image presents the original (without segmentation) and the results (with segmentation). The ground truth boundary and the segmented boundary are shown as well.

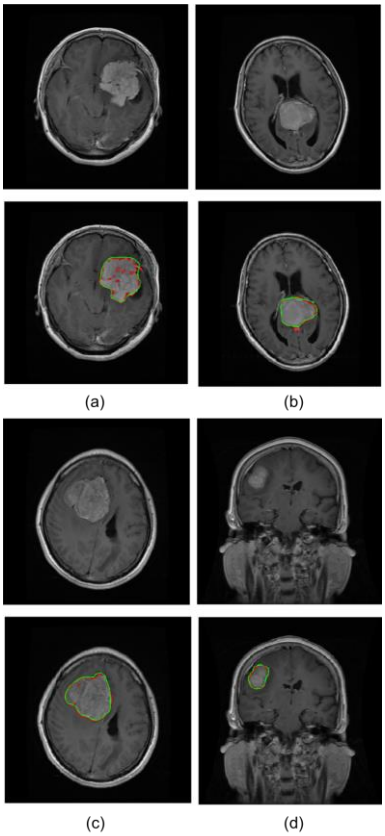

Fig. 4.1. Segmentation of Meningioma tumor, top row indicates original images, and the bottom row shows the results of segmentation for 3.png (a), 22.png (b), 75.png (c), 274.png (d). The Redline is a segmented boundary tumor, and the green line is the boundary of the ground truth of tumor images.

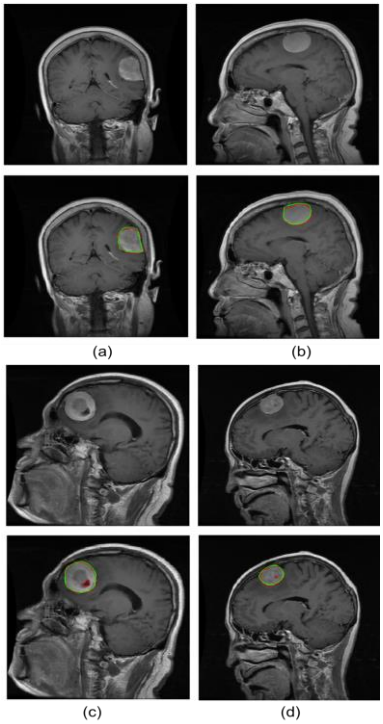

Fig. 4.2. Segmentation of Meningioma tumor, top row indicates original images and bottom row indicates the results of segmentation for 279.png (a), 521.png (b), 524.png (c), 690.png (d). The red line is a segmented boundary tumor, and the green line is the boundary of the ground truth of tumor images.

The results in Fig. 4.1 – Fig. 4.2 show that the Phase Field method can segment the Meningioma tumor in each medical image. The difference between the ground truth boundary and the segmented boundary is comparable.

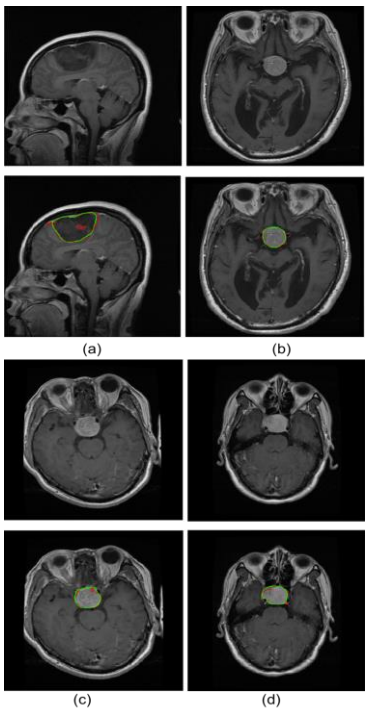

Fig. 5.1. Segmentation of Pituitary tumor, top row indicates original images and bottom row indicates the results of segmentation for 887.png (a), 922.png (b), 935.png (c), 995.png (d). The red line is a segmented boundary tumor, and the green line is the boundary of the ground truth of tumor images.

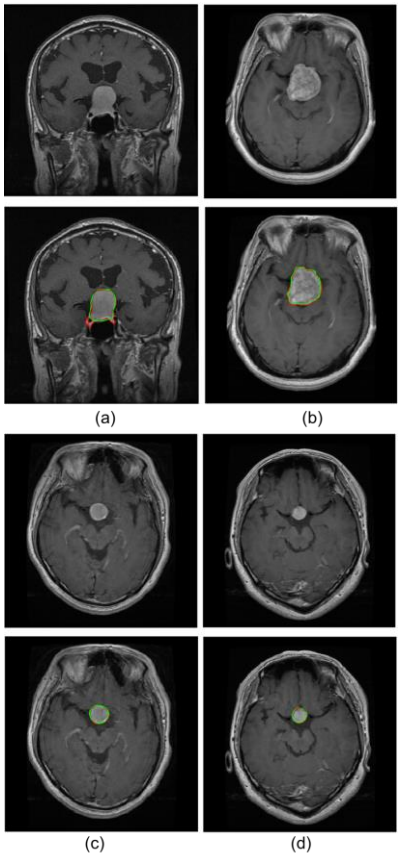

Fig. 5.2. Segmentation of Pituitary tumor, top row indicates original images and bottom row indicates the results of segmentation for 1039.png (a), 1357.png (b), 1428.png (c), 1454.png (d). The red line is the boundary of the segmented tumor, and the green line is the boundary of the ground truth of tumor images

In the case of segmenting the Pituitary tumor, the results in Fig. 5.1 – Fig. 5.2 proves that the Phase Filed method can segment the tumor. As can be seen, the difference between the ground truth boundary (green line) and the segmented boundary (red line) of the Pituitary tumor is relatively similar. Based on the results in Fig. 4.1 – Fig. 4.2 and Fig. 5.1 – 5.2, it is evident that the segmentation process using the Phase Field method for Meningioma tumor and Pituitary tumor have a good match with the ground truth boundary in the dataset. Furthermore, Table 2 and Table 3 show the qualitative evaluation of Meningioma and Pituitary tumor segmentation results using the Jaccard Index and Dice Similarity.

TABLE II
QUALITATIVE EVALUATION OF SEGMENTATION RESULTS OF MENINGIOMA TUMOR

No	Testing Images	Jaccard Index	Dice Similarity
1	3.png	0.875	0.936
2	22.png	0.918	0.959
3	75.png	0.948	0.974
4	274.png	0.900	0.949
5	279.png	0.921	0.960
6	521.png	0.859	0.926
7	524.png	0.909	0.955
8	690.png	0.899	0.949

TABLE III
QUALITATIVE EVALUATION OF SEGMENTATION RESULTS OF PITUITARY TUMOR

No	Testing Images	Jaccard Index	Dice Similarity
1	887.png	0.919	0.960
2	922.png	0.952	0.976
3	935.png	0.927	0.964
4	995.png	0.912	0.957
5	1039.png	0.889	0.948
6	1357.png	0.944	0.972
7	1428.png	0.936	0.936
8	1454.png	0.922	0.960

Based on Table II and Table III, the Jaccard Index and Dice Similarity are relatively high. The minimum value of the Jaccard Index in the case of the Meningioma tumor is 0.859, and the Pituitary tumor is 0.889. In terms of Dice Similarity, the minimum value in the case of the Meningioma tumor is 0.926 and the Pituitary tumor is 0.936. If the Jaccard Index and Dice Similarity value is high and closer to 1, the two images are highly similar. As the Jaccard Index and Dice Similarity achieved in each image is high; therefore, the results have high accuracy.

V. CONCLUSION

This paper proposes using the Phase Filed method using the second-order Ringe-Kutta method and parallels GPU programming for medical image segmentation. After comparing the segmentation of sample images taken from the benchmark dataset with the ground truth dataset, the Phase Field method has high accuracy. The high accuracy of the Phase Filed method is indicated by the Jaccard Index and Dice Similarity value, which is close to number one. The range of Jaccard Index values is 0.859 - 0.952, while the range of Dice Similarity values is 0.926 - 0.976. Furthermore, based on the experiments, when compared to serial programming with the CPU, GPU CUDA-based parallel programming can greatly reduce the elapsed time of the segmentation process. In this research, parallel programming with GPU CUDA accelerated 45.72 times than serial programming with the CPU.

Based on the research that has been done in this paper, several suggestions can be carried out in further research, such as adding advection terms to the model equation that can move the level curve faster and selecting the right criteria for the evaluation of segmentation results needs to be studied further.

REFERENCES

[1] A. W. Rosyadi and N. Suciati, "Image Segmentation Using Transition Region and K K-Means Clustering," IAENG International Journal of Computer Science, vol. 47, no. 1, pp.47-55, 2020.

[2] N. Mohd Saad, N. S. M. Noor, A.R. Abdullah, Sobri Muda, A. F. Muda, and H. Musa, "Segmentation and Classification Analysis Techniques for Stroke based on Diffusion-Weighted Images," IAENG International Journal of Computer Science, 44:3, pp. 388-395, 2017.

[3] P.K.R. Yelampalli, J. Nayak, and V.H. Gaidhane, "Blood Vessel Segmentation and Classification of Diabetic Retinopathy Images using Gradient Operator and Statistical Analysis," Proceedings of the World Congress on Engineering and Computer Science 2017 Vol II, WCECS 2017, October 25-27, 2017, San Francisco, USA.

[4] M. Kass, A. Witkin, and D.Terzopolous, "Snakes: active contour models," International Journal of Computer Vision, vol. 1, no. 4, pp. 321–331, 1988.

[5] S. Osher and J.A. Sethian, "Fronts propagating with curvature-dependent speed: algorithms based on Hamilton–Jacobi formulations, " Journal of Computational Physics, vol. 79, no, 1, pp. 12–49, 1988.

[6] T. Chan and L.A. Vese, "Active contours without edges," IEEE Transactions on Image Processing, vol.10, no. 2, pp. 266–277, 2001.

[7] D. Mumford and J. Shah, "Optimal approximation by piecewise smooth functions and associated variational problems," Communications on Pure and Applied Mathematics, vol. 42, no, 5, pp. 577–685, 1989.

[8] M. Maška, O. Daněk, S. Garcia, A. Rouzaut, A. M. Muñoz-Barrutia, and C. Ortiz-de-Solorzano, "A Segmentation and Shape Tracking of Whole Fluorescent Cells Based on the Chan–Vase Model," IEEE Transactions on Medical Imaging, vol. 32, no. 6, pp. 995-1006, 2013.

[9] Y. Chen, Y. Liu, and X. Zhu, "Robust iris segmentation algorithm based on self-adaptive Chan–Vese level set model," Journal of Electronic Imaging, vol. 24, no. 4, pp. 043012-1 - 043012-12, 2015.

[10] S. Rajalaxmi and S. Nirmala, "Automated Endo Fitting Curve for Initialization of Segmentation Based on Chan Vase Model," Journal of Medical Imaging and Health Informatics, vol. 5, no. 3, pp. 572–580, 2015.

[11] M. A.Femina and S. P. Raajagopalan, "Anatomical structure segmentation from early fetal ultrasound sequences using global pollination CAT swarm optimizer–based Chan–Vese model," Medical & Biological Engineering & Computing, vol. 57, no. 8, pp. 1763-1782, 2019.

[12] M. Beneš, V. Chalupecký, and K. Mikula, "Geometrical image segmentation by the Allen–Cahn equation," Applied Numerical Mathematics, vol. 51, no. 2-3pp. 187–205, 2004.

[13] D.A. Kay and A. Tomasi, Color Image Segmentation by the Vector-Valued Allen–Cahn Phase-Field Model: A Multigrid Solution, IEEE Transactions on Image Processing, vol. 18, no. 10, 2009.

[14] Y. Li and J.S. Kim, "A fast and accurate numerical method for medical image segmentation," Journal of The Korean Society for Industrial and Applied Mathematics, vol. 14, no. 4, pp. 201-210, 2010.

[15] Y. Li and J.S. Kim, "An unconditionally stable hybrid method for image segmentation," Applied Numerical Mathematics, vol. 82, no. 3, pp. 32–43, 2014.

[16] Y. Li and J.S. Kim, "Multiphase image segmentation using a phase-field model," Computers and Mathematics with Applications, vol. 62, no. 2, pp. 737–745, 2011.

[17] A. A. H. Thasneem, M. Mohamed Sathik, and R. Mehaboobathunnisa, "A Fast Segmentation and Efficient Slice Reconstruction Technique for Head CT Images," Journal of Intelligent Systems, vol 28, no. 4, pp. 533–547, 2017.

[18] Lee, D. and Lee, S., "Image Segmentation Based on Modified Fractional Allen–Cahn Equation," Mathematical Problems in Engineering, vol.2019, Article ID 3980181, 2019.

[19] C. Zhu, J. Jia, H. Zhang, R. Xiao, and L. Feng, "Parallel Implementation for Phase-Field Simulation of Flow Effect on Dendritic Growth with GPU Acceleration," Materials Transactions, vol. 55, no. 12, pp. 1841-1846, 2014.

[20] C.Yang, Q.Xu, and B.Liu, "GPU-accelerated three-dimensional phase-field simulation of dendrite growth in a nickel-based superalloy," Computational Materials Science, vol. 136, no. 16, pp. 133–143, 2017.

[21] J.Lee and K.Chang, "Effect of magnetic ordering on the spinodal decomposition of the Fe-Cr system: A GPU-accelerated phase-field study," Computational Materials Science, vol. 169 109088, 2019.

[22] S. C. Chapra and R. P. Canale, "Numerical Methods for Engineers", McGraw-Hill Higher Education, New York, USA, sixth edition, 2009.

[23] J. Cheng, M. Grossman, and T. McKercher, "Professional CUDA C Programming", Wrox, John Wiley & Sons, Inc., Indianapolis, USA, 2014.

[24] I.B. Suban, Suyoto, and Pranowo, "Medical Image Segmentation Using a Combination of Lattice Boltzmann Method and Fuzzy Clustering Based on GPU CUDA Parallel Processing", International Journal of Online and Biomedical Engineering (iJOE), 2021

[25] J. Lai, H. Li, Z. Tian, and Y. Zhang, "A Multi-GPU Parallel Algorithm in Hypersonic Flow Computations," Mathematical Problems in Engineering, vol. 2019, Article ID 2053156, 2019.

[26] J. Cheng, W. Huang, S. Cao, R. Yang, W. Yang, Z. Q. Yun, Z. Wang, and Q. Feng, "Enhanced Performance of Brain Tumor Classification via Tumor Region Augmentation and Partition," PLoS ONE, vol. 10, no. 12, pp. 1-13, 2015.

[27] J. Cheng, W. Yang, M. Huang, W. Huang, J. Jiang, Y. Zhou, R. Yang, J. Zhao, Y. Feng, Q. Feng, and W. Chen, "Retrieval of Brain Tumors by Adaptive Spatial Pooling and Fisher Vector Representation," PLoS ONE, vol. 11, no. 6, pp. 1-15, 2016.

[28] T. Eelbode et al., "Optimization for Medical Image Segmentation: Theory and Practice When Evaluating With Dice Score or Jaccard Index," IEEE Transactions on Medical Imaging, vol. 39, no. 11, pp. 3679-3690, 2020.